[AMERICAN JOURNAL OF SCIENCE, SCHAIRER VOL. 267-A, 1969, P. 342-363]

THE SYSTEM MgO–SiO_2–TiO_2 AND ITS BEARING ON THE DISTRIBUTION OF TiO_2 IN BASALTS*

IAN D. MacGREGOR

Southwest Center for Advanced Studies, Box 30365
Dallas, Texas 75230

ABSTRACT. Experimental determination of the liquidus and solidus relationships in the Mg_2SiO_4–Mg_2SiO_3–TiO_2–$MgTi_2O_5$ portion of the system MgO–SiO_2–TiO_2, with a solid-media, piston-cylinder device, indicate that the following univariant reactions occur between 1 atm and 40 kb:

$$En + M = Fo + 2Rt \quad (1)$$
$$L_2 = Fo + En + M \quad (2)$$
$$L_3 + Fo = M + En \quad (3)$$
$$L_4 = M + En + Rt \quad (4)$$
$$L_5 + M = Fo + Rt \quad (5)$$
$$L_6 = Fo + En + Rt \quad (6)$$
$$L_7 = M + Fo + Rt \quad (7)$$

(where $En = MgSiO_3$, $M = MgTi_2O_5$, $Fo = Mg_2SiO_4$, $Rt = TiO_2$, L_n = liquid). The compositions of the liquids 2 through 7 become progressively more TiO_2-rich and MgO- and SiO_2-poor with increasing pressure. Reactions (1), (3), (4), (5), and (6) intersect at an invariant point at 1489°C and 15.2 kb.

The results of discriminant function analysis suggests that TiO_2 is by far the best oxide in distinguishing between Cenozoic basalts from oceanic island and circumoceanic localities. However, model ultramafic compositions in the system, MgO–SiO_2–TiO_2, give rise to successively TiO_2-rich partial fusion products with increasing pressure, suggesting a qualitative analogy that basaltic magmas are progressively enriched in TiO_2 the greater their depth or origin. Comparison of the experimental compositions with those of Cenozoic basalts suggests that the successful geographic division into oceanic island and circumoceanic environments is related more to the tectonic setting than regional geochemical variations.

INTRODUCTION

Recent studies (Chayes, 1964; Chayes and Velde, 1965) have examined the interrelationship of the two factors, geography and chemistry, in the genesis and history of basalts. These authors have shown that TiO_2 is the most useful single oxide for distinguishing circumoceanic from oceanic-island Cenozoic basalts. Linear combinations of one, two, and three additional oxides with TiO_2 show only slight increases in discriminatory efficiency. Furthermore, binary and ternary combinations that exclude TiO_2 show a marked decrease in discriminatory efficiency. The most efficient discriminant between rocks from the two geographic settings is the ternary combination MgO–SiO_2–TiO_2.

From the statistical analysis (Chayes and Velde, 1965), therefore, the ternary system, MgO–SiO_2–TiO_2, may be chosen as a simple and likely system, from which an understanding of the distribution of TiO_2 in basaltic rocks can be deduced by laboratory experiment. Compositions in this ternary system also have the realistic feature that they may be approximately regarded as model ultramafic compositions. The probability that the upper mantle is ultramafic in composition (Green and Ringwood, 1963; Ringwood, 1966; Carter, 1966; Hess, 1964; Harris, Reay, and White, 1967) and the hypothesis that basalts are derived as

* Contribution no. 72, Geoscience Division, Southwest Center for Advanced Studies, Box 30365, Dallas, Texas 75230

partial melts of mantle rocks (Yoder and Tilley, 1962; Green and Ringwood, 1967) give added appeal to this simple model. In as much as the genesis and evolution of basalts probably result from complex processes involving partial melting and fractional crystallization at different depths within the crust and mantle, it is obvious that pressure is a variable whose importance must be evaluated.

Accordingly a study was undertaken to determine experimentally the effect of pressure on the solidus and liquidus relationships in that part of the ternary system, MgO–SiO_2–TiO_2, pertinent to basalt genesis. The subsolidus regions of interest are the ternary Mg_2SiO_4–$MgSiO_3$–$MgTi_2O_5$ at low pressures and Mg_2SiO_4–$MgSiO_3$–TiO_2 at high pressures. Model ultramafic compositions contain a small amount of TiO_2 and lie close to the tie-line Mg_2SiO_4–$MgSiO_3$ (fig. 1). The isobaric liquidus surfaces provide a test of the effect of such processes as partial melting and fractional crystallization at different depths on the composition of model basalts in the simple ternary.

EXPERIMENTAL RESULTS

Subsolidus relationships.–The following phases are present in the subsolidus region: periclase (MgO), magnesium orthotitanate (Mg_2TiO_4), giekielite ($MgTiO_3$), magnesium titanate ($MgTi_2O_5$), rutile (TiO_2), forsterite (Mg_2SiO_4), enstatite ($MgSiO_3$), and quartz or coesite (SiO_2) (fig. 1). The phases $MgTi_2O_4$, $MgTiO_3$, $MgTi_2O_5$, Mg_2SiO_4, and $MgSiO_3$ are not found as pure minerals in nature. However, they do occur as components, with Fe^{++}-bearing analogs, in the ulvospinel, ilmenite, olivine, and orthopyroxene solid solution series.

Although, not examined in detail, the experimental data do indicate that there is very little solid solution between the phases examined. This observation is supported by analytical data on natural mineral equivalents from a wide range of basalts from different geological environments, which suggest that there is essentially no solid solution between the different solid phases in the experimental range examined.

Within the four-phase region Mg_2SiO_4–$MgSiO_3$–TiO_2–$MgTiO_3$, the only subsolidus reaction found to occur, within the pressure-temperature range investigated, is the following:

$$MgSiO_3 + MgTi_2O_5 = Mg_2SiO_4 + 2TiO_2 \qquad (1)$$

The pressure-temperature dependence of reaction (1) (fig. 2, table 1) may be described by the equation

$$T = 32.46\ P + 996$$

(where P is in kb and T in °C). In determining this curve, starting materials were made up of crystalline mixtures characteristic of each side of equation (1). The high-pressure assemblage was held at one temperature, at successively lower pressures. The reaction boundary was recorded above that pressure where the low-pressure assemblage first appeared in the products. The same procedure using successively higher pressures was used for the low-pressure starting material, and the boundary recorded below the first appearance of the high-pressure assemblage

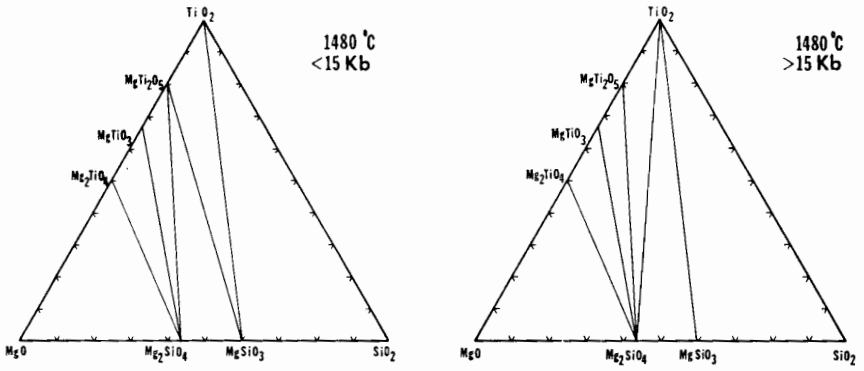

$MgSiO_3 + MgTi_2O_5 \rightleftharpoons Mg_2SiO_4 + 2TiO_2$

Fig. 1. Subsolidus phase fields at 1480°C from 1 atm to 40 kb.

in the products. In this way a reversed boundary was recorded at 1200, 1400, and 1500°C (fig. 2).

The 1 atm liquidus surface.—The liquidus surface at 1 atm pressure (fig. 4A) has previously been determined (Massazza and Sirchia, 1958b). A cursory study of the join $MgSiO_3$–TiO_2 by J. F. Schairer (personal commun., 1964) showed that the eutectic temperature is probably about 10° lower than previously indicated (Massazza and Sirchia, 1958a), but the eutectic composition seems approximately correct. There are two eutectic liquids (E_2 and E_4, fig. 4A) defined by the reactions

$$L_2 = Fo + En + M \quad (2)$$

and

$$L_4 = M + En + Rt \quad (4)$$

(where Fo = Mg_2SiO_4, En = $MgSiO_3$, Rt = TiO_2, and M = $MgTi_2O_5$). The compositions of L_2 and L_4 are given in table 6.

The 10 kb liquidus surface.—The liquidus surface at 10 kb (fig. 4B) was constructed from data on the joins $MgSiO_3$–TiO_2, Mg_2SiO_4–TiO_2 and $MgSiO_3$–$MgTi_2O_5$ (fig. 3D, E, and F; tables 2, 3, and 4) and from compositions close to the peritectic and eutectic (table 5). At 10 kbs there is a peritectic (P_3) and eutectic (E_4) (fig. 4B) defined by equations (3) and (4)

$$L_3 + Fo = M + En \quad (3)$$

The peritectic composition is determined by the intersection of the lines through the projected peritectic compositions, on the two joins Mg_2SiO_4–TiO_2 (fig. 3E) and $MgSiO_3$–$MgTi_2O_5$ (fig. 3F), from $MgTi_2O_5$ and Mg_2SiO_4, respectively. The ternary eutectic composition is determined with the aid of the projection through the eutectic composition on the join Mg_2SiO_4–TiO_2 from $MgTi_2O_5$, and from an examination of compositions close to the eutectic (table 5). The composition of the peritectic (P_3)and the eutectic (E_4) is given in table 6.

TABLE 1

Experimental results for the reaction $MgSiO_3 + MgTi_2O_5 \rightleftharpoons Mg_2SiO_4 + 2TiO_2$

Composition, weight percent		Pressure, kb	Temp, °C	Time, min	Starting material*	Products*
Mg_2SiO_4	TiO_2					
80	20	10	1475	60	Fo + Rt	En + M + Fo + Rt
46.73	53.26	12.5	1500	30	Fo + Rt	En + M
46.73	53.26	15	1500	44	Fo + Rt	En + M + (Fo) + (Rt)
46.73	53.26	17.5	1500	45	En + M	Fo + Rt + (M)
46.73	53.26	20	1500	45	En + M	Fo + Rt
60	40	20	1550	30	En + M	Fo + Rt + ((Q))
46.73	53.26	10	1400	60	Fo + Rt	En + M + (Fo) + (Rt)
46.73	53.26	12.5	1400	90	En + M	Fo + Rt + (En) + (M)
46.73	53.26	15	1400	65	En + M	Fo + Rt
46.73	53.26	5	1200	720	Fo + Rt	En + M + (Fo) + (Rt)
46.73	53.26	7.5	1200	180	En + M	Fo + Rt + (En) + (M)
46.73	53.26	10	1200	180	En + M	Fo + Rt + (En) + (M)
43	57	12.5	1200	180	En + M	Fo + M + (En)

*Abbreviations: Fo, forsterite; En, enstatite; M, magnesium titanate; Rt, rutile; Q, quench crystals; parentheses indicate minor amounts; double parentheses indicate trace amounts; underline indicates subsolidus assemblage.

The 15.5 kb liquidus surface.—The liquidus surface at 15.5 kb was constructed from data on the joins Mg_2SiO_4–TiO_2 and $MgSiO_3$–$MgTi_2O_5$ (figs. 3H and I; tables 3 and 4), and from a few compositions not on these joins (table 5). The liquidus on the join $MgSiO_3$–TiO_2 (fig. 3G) was interpolated from data obtained at 10 and 20 kb (table 2). On the join $MgSiO_3$–$MgTi_2O_5$ (fig. 3I) the phase field $Mg_2SiO_4 + TiO_2 +$ liquid must have a width less than 5°C. Because of the thermal gradient across the sample (±10°C) it was not possible to make an experiment completely within this field. However, in two experiments (table 4) the products showed assemblages which straddled 3 phase fields, that is, $MgTi_2O_5 + Mg_2SiO_4 +$ liquid, $Mg_2SiO_4 +$ liquid, and $Mg_2SiO_4 + MgSiO_3 + TiO_2$. The existence and width of the $MgSiO_4 + TiO_2 +$ liquid phase field (fig. 3I) was deduced from these results. At 15.5 kb there is a peritectic (P_5) and eutectic (E_6) (fig. 4C), which are defined respectively, by equations (5) and (6)

$$L_5 + M = Fo + Rt, \tag{5}$$

and

$$L_6 = Fo + En + Rt \tag{6}$$

The peritectic (P_5) (fig. 4C) lies at the intersection of the two lines through the projected peritectic compositions, on the joins $MgSiO_3$–$MgTi_2O_5$ and Mg_2SiO_4–TiO_2, from Mg_2SiO_4 and $MgTi_2O_5$, respectively. Assuming no solid solution, the location of the eutectic (E_6) may be determined by the line joining the projected eutectic composition on the join $MgSiO_3$–$MgTi_2O_5$ (fig. 3I) to Mg_2SiO_4, plus additional data from compositions close to the eutectic (table 5). The compositions of the peritectic (P_5) and eutectic (E_6) at 15.5 kb are shown in table 6.

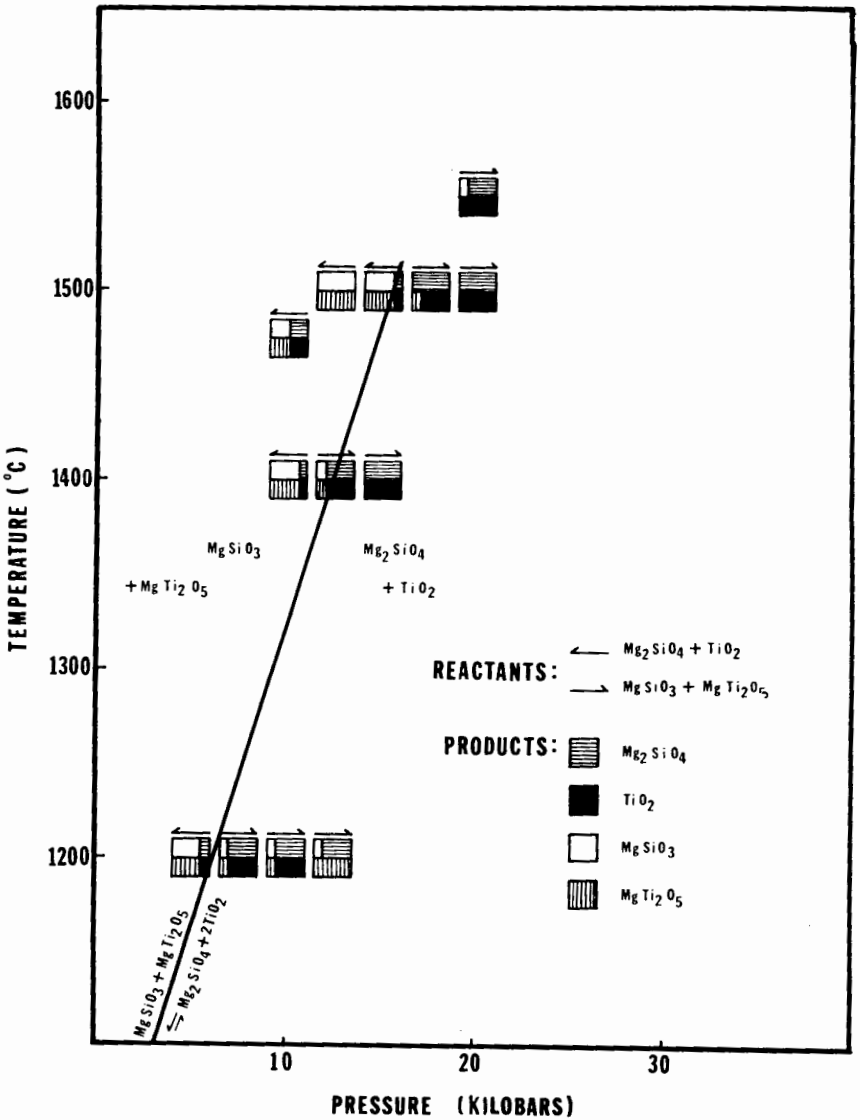

Fig. 2. Temperature-pressure section showing experimental determination of univariant subsolidus reaction $MgSiO_3 + MgTi_2O_5 = Mg_2SiO_4 + TiO_2$.

The 20 kb liquidus surface.—The liquidus surface at 20 kbs (fig. 4D) was constructed from data on the joins $MgSiO_3$–TiO_2, Mg_2SiO_4–TiO_2, and $MgSiO_3$–$MgTi_2O_5$ (fig. 3J, K, and L; tables 2, 3, and 4) and from other compositions in the ternary diagram (table 5). At 20 kbs there is a peritectic (P_5) and eutectic (E_6) defined by equations (5) and (6).

Assuming no solid solution, the peritectic (P_5) lies at the intersections of the lines, from Mg_2SiO_4 and $MgTi_2O_5$, through the projected peritectic compositions on the joins Mg_2SiO_4–TiO_2 and $MgSiO_3$–$MgTi_2O_5$, respectively. The ternary eutectic (E_2) was located with the aid of the projection, from Mg_2SiO_4, through the eutectic composition on the join $MgSiO_3$–$MgTi_2O_5$, and by examining ternary compositions close to the eutectic. The compositions of the peritectic (P_5) and eutectic (E_6) at 20 kb are shown in table 6.

The 40 kb liquidus surface.—The liquidus surface at 40 kb (fig. 4E) was constructed from data on the joins $MgSiO_3$–TiO_2, Mg_2SiO_4–TiO_2, and $MgSiO_3$–$MgTi_2O_5$ (fig. 3M, N, and O; tables 2, 3, and 4) and from a few other compositions not on these joins (table 5). At 40 kb there are two eutectics (E_6 and E_7) defined by reactions (6) and (7)

$$L_7 = M + Fo + Rt. \quad (7)$$

Assuming no solid solution, the eutectic compositions (E_6 and E_7) may be located with the aid of projections, from Mg_2SiO_4, through the projected eutectic compositions on the join $MgSiO_3$–$MgTi_2O_5$, plus additional data in the ternary diagram (table 5). The compositions of the eutectics (E_6 and E_7) at 40 kb are shown in table 6.

The invariant point.—There is one invariant point in the Mg_2SiO_4–$MgSiO_3$–TiO_2–$MgTi_2O_5$ portion of the ternary system (fig. 5). This point is defined by the intersection of the reactions

$$En + M = Fo + Rt \quad (1)$$
$$L_3 + Fo = M + En \quad (3)$$
$$L_4 = M + En + Rt \quad (4)$$
$$L_5 + M = Fo + Rt \quad (5)$$
$$L_6 = Fo + En + Rt \quad (6)$$

The data for reaction (1) are from table 1 and for reactions (3), (4), (5) and (6), from table 6. The invariant point occurs at 15.2 kb and 1489°C. The composition of the invariant liquid is given in table 6. Reactions (2) and (7) (fig. 5) represent the univariant equilibria for the eutectics (E_2 and E_7) which do not intersect at the variant point, since they become peritectic (P_3 and P_5) reactions at 6.4 and 35.6 kb, respectively.

Change of ternary liquidus surface with pressure.—In the Mg_2SiO_4–$MgSiO_3$–$MgTi_2O_5$–TiO_2 portion of the ternary system there are significant changes in the ternary liquidus surface as a function of pressure (fig. 4A, B, C, D, and E). These changes may best be examined by following the traces of the peritectics and eutectics defined by the reactions (2) through (7) (fig. 4F).

At 1 atm there are two eutectics (E_2 and E_4) (fig. 4F). With increasing pressure, the eutectics, E_2 and E_4, migrate to increasingly TiO_2-rich compositions. At approximately 6.4 kb the eutectic, E_2, changes to a peritectic, P_3. Both the peritectic (P_3) and eutectic (E_4) liquids become increasingly TiO_2-rich through 10 kb till they merge at the invariant point at 15.2 kb. At pressures above the invariant point there are new peritectic (P_5) and eutectic (E_6) liquids. These two liquids migrate

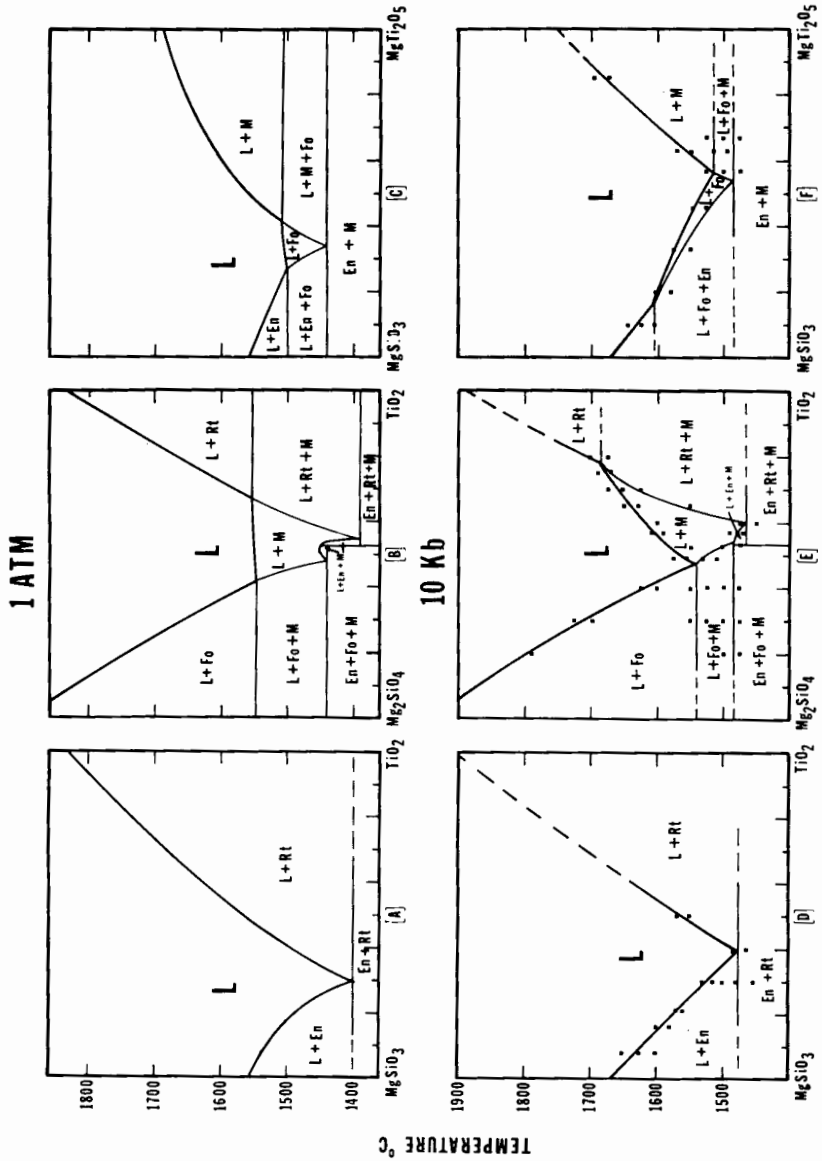
1 ATM
10 Kb
TEMPERATURE °C
WEIGHT PER CENT
L
L+En
L+Rt
En+Rt
L+Fo
L+M
L+Rt+M
En+Fo+M
L+En+Fo
L+En+M
L+Fo+M
L+Fo+En
L+Fo+M
En+Rt+M
En+M
L+M+Fo
L+Fo+M
[A]
[B]
[C]
[D]
[E]
[F]
$MgSiO_3$
Mg_2SiO_4
$MgSi_2O_5$
TiO_2
1400
1500
1600
1700
1800
1900

Fig. 3.

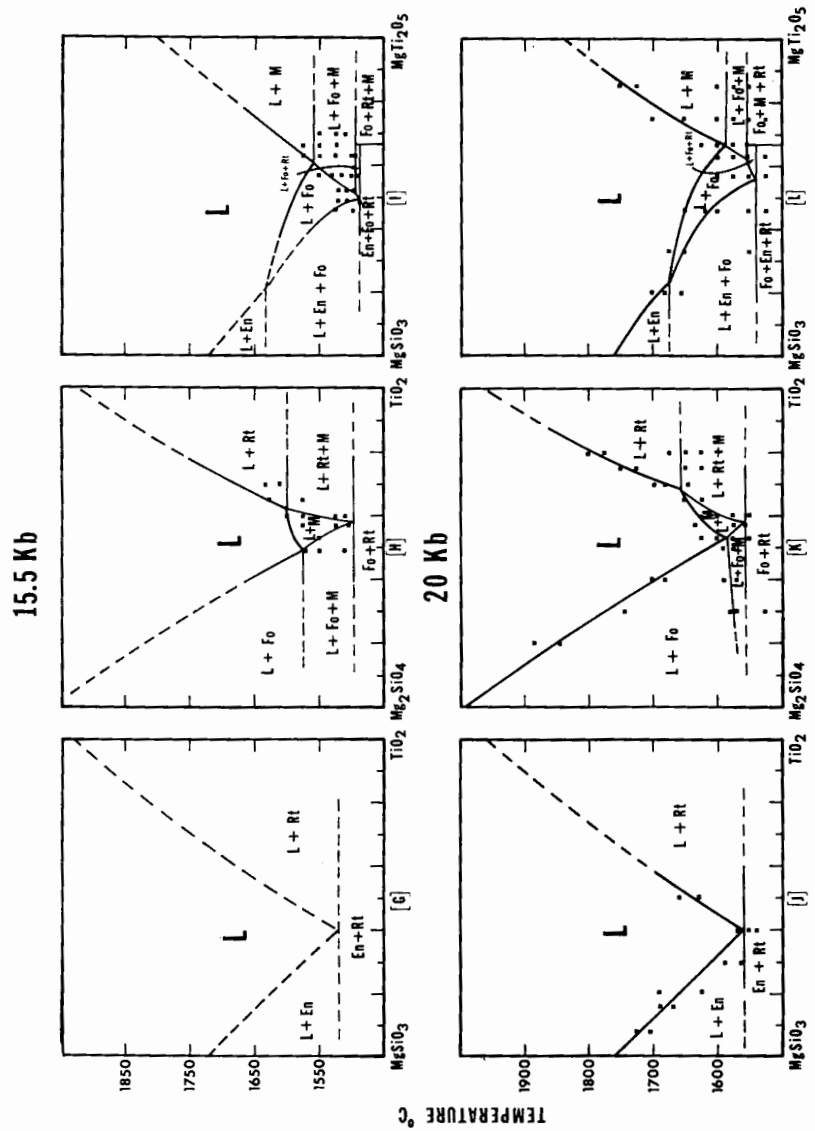

Fig. 3. (Continued)

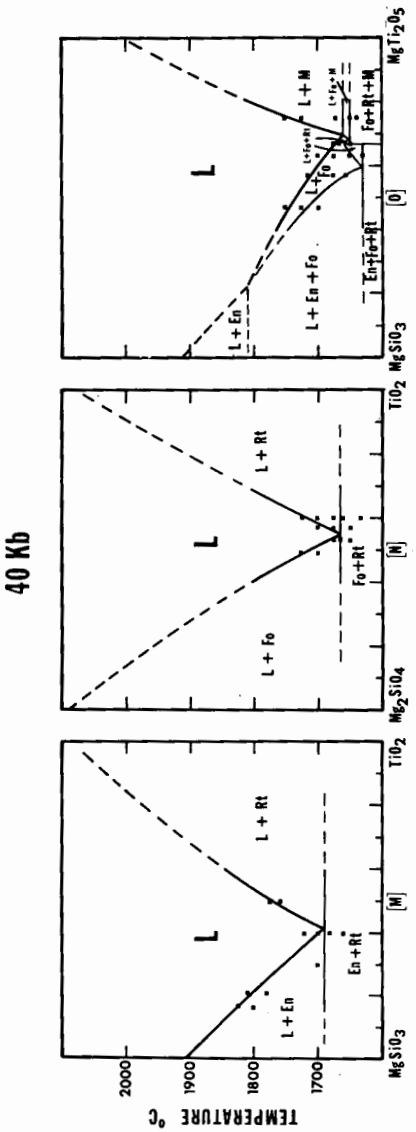

Fig. 3. (Continued)

Fig. 3A to O. Binary sections through the ternary system (solid squares give data points listed in tables 2, 3, and 4).

toward $MgTi_2O_5$ with increasing pressure through 15.5 and 20 kb. Between 20 and 40 kb a similar trend is observed, but at approximately 35.6 kb the peritectic (P_5) turns into a eutectic (E_7).

The main effect of pressure in this system is to increase the TiO_2 content of all eutectic and peritectic liquids (fig. 4F). In general, the MgO and SiO_2 content decrease with increasing pressure. It should be noted that nearly all the variation occurs in the pressure range below 20 kb. Only slight changes of composition occur in the pressure range 20 to 40 kb.

TABLE 2

Experimental results on the join $MgSiO_3$-TiO_2

Composition, weight percent		Temp, °C	Pressure, kb	Time, min	Starting material*	Products*
$MgSiO_3$	TiO_2					
91.4	8.6	1650	10	15	En + Rt	G
91.4	8.6	1625	10	15	En + Rt	En + Q
91.4	8.6	1600	10	20	En + Rt	En + Q
83.4	16.6	1600	10	13	En + Rt	G + Q + (En)
83.4	16.6	1580	10	20	En + Rt	En + G + Q
79.1	20.9	1570	10	28	G + Q	Q + (G)
79.1	20.9	1560	10	14	G + Q	En + G
70	30	1525	10	35	G + Q	Q
70	30	1515	10	20	G + Q	En + Q
70	30	1500	10	30	G + Q	En + Q
70	30	1480	10	25	G + Q	En + Q
70	30	1455	10	40	G + Q	En + Rt
60	40	1480	10	25	G + Q	Q + (Rt)
60	40	1465	10	30	G + Q	En + Rt
50	50	1570	10	20	En + Rt	Q + (Rt)
50	50	1550	10	25	En + Rt	Q + Rt
91.4	8.6	1725	20	7	En + Rt	G + Q
91.4	8.6	1705	20	11	En + Rt	Q + En
83.4	16.6	1690	20	15	En + Rt	Q + (En)
83.4	16.6	1670	20	15	En + Rt	Q + En
79.1	20.9	1690	20	15	G + Q	Q + (En)
79.1	20.9	1625	20	15	G + Q	Q + En
70	30	1590	20	20	G + Q	Q + En
70	30	1565	20	15	G + Q	Q + En
60	40	1565	20	23	G + Q	Q
60	40	1555	20	20	G + Q	En + Rt
60	40	1540	20	20	G + Q	En + Rt
50	50	1660	20	10	En + Rt	Q
50	50	1630	20	5	En + Rt	Q + Rt
83.4	16.6	1825	40	2	En + Rt	Q
83.4	16.6	1800	40	2	En + Rt	Q + Fo
79.1	20.9	1810	40	2	G + Q	Q
79.1	20.9	1780	40	3	G + Q	Q + Fo
70	30	1700	40	3	G + Q	Q + Fo
60	40	1720	40	3	G + Q	Q
60	40	1700	40	3	G + Q	Q + Fo
60	40	1680	40	3	G + Q	Fo + Rt
50	50	1775	40	2	En + Rt	Q
50	50	1760	40	2	En + Rt	Q + Rt

*Abbreviations: Fo, forsterite; En, enstatite; Rt, rutile; Q, quench crystals; G, glass; parentheses indicate minor amounts; underline indicates subsolidus assemblage.

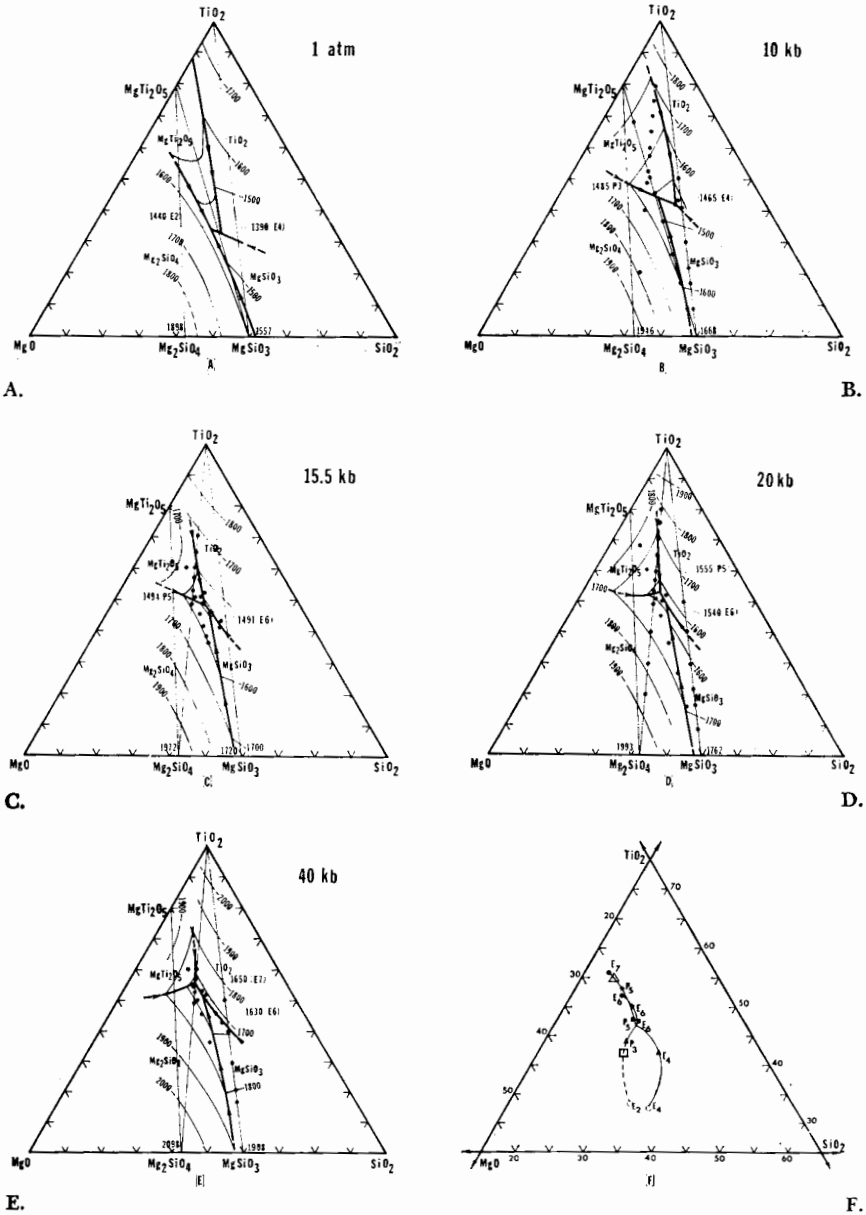

Fig. 4A to E. Ternary liquidus surface at 1 atm (Massazza and Sirchia, 1958b) and 10, 15.5, 20, and 40 kb. (solid dots give data points, heavy lines are boundary curves, intermediate lines are isotherms, light lines define subsolidus phase fields).

F. Summary of the change of composition of ternary peritectics (P_3 and P_5) and ternary eutectics (E_2, E_4, E_6, and E_7) with pressure. Open circle, 1 atm; solid triangle, 10 kb; solid square, 15.5 kb; solid star, 20 kb; solid circle, 40 kb; open square, interpolated point at 4.6 kb; open triangle, interpolated point at 35.6 kb.

PETROLOGICAL APPLICATIONS

As with any experimental investigation of an idealized simple system, there are problems in applying the results to far more complex natural systems. In nature, other components such as iron exist in solid solution in nearly all the phases represented in the ternary system, and Ca is an important component of the pyroxene and titanate phases. The components, Al_2O_3, Na_2O, and K_2O also have important roles in the genesis of basalts and along with FeO, Fe_2O_3, and CaO form additional phases not present in the ternary system. Further, the TiO_2 is rarely and $MgTi_2O_5$ never found as primary phases in volcanic rocks. Despite these considerations it is possible to make a few qualitative statements about the broad question of the genesis of basalts.

The small molar volume of TiO_2, relative to other basalt phases, will probably lead to reactions that, with increasing pressure, will stabilize subsolidus phase assemblages coexisting with rutile. This tendency, in conjunction with a preliminary value of 6 $\pm$ 2°C per kb for the slope of the melting curve of TiO_2 (estimated from the extrapolated liquidus curves on the $MgSiO_3$–TiO_2 and Mg_2SiO_4–TiO_2 joins in fig. 3), when compared with values of 15.4, 14, 12.5 and 4.77°C per kb for diopside, albite (Boyd and England, 1963), enstatite (Boyd, England and Davis, 1964), and forsterite (Davis and England, 1964), respectively, indicates that the minimum melting compositions of ultramafic rocks will in general migrate toward rutile and forsterite with increasing pressure. This trend will probably decrease with increasing pressure since the slope of the melting curves for basaltic minerals decreases to approximately 6°C per kb at about 30 kb. This effect is well-illustrated in the ternary system where only slight changes in eutectic and peritectic composition are observed in the pressure range 20 to 40 kb, whereas there are significant compositional changes from 1 atm to 20 kb (fig. 4F).

The important qualitative observation that may be made from the experimental results is that the TiO_2 content of liquids, derived from a peridotitic parent, will increase with increasing pressure. The nature of the compositional changes with pressure, viz. a rapid change in the pressure range 1 atm to 20 kb with very minor changes in the 20 to 40 kb range (fig. 4F), is also significant. It is apparent that bimodal distributions of TiO_2 could readily be obtained from the above compositional variations. Peak values at high TiO_2 contents would indicate a genesis at higher pressures than a set of TiO_2 contents at lower values. Extrapolation of the experimental data to Chayes' (1964) observations suggests that the basalts with TiO_2 values in the lower peak are derived from lower pressures than basalts with TiO_2 values in the higher peak, that is, the circumoceanic basalts are generally derived from shallower depths than the oceanic island basalts. The greater proportion of basalts with lower TiO_2 contents also suggests that most Cenozoic basalts are either derived from shallower depths or reflect a major imprint on their chemistry of a lower pressure fractional crystallization stage in their history.

TABLE 3

Experimental results on the join Mg_2SiO_4-TiO_2

Composition, weight percent		Temp, °C	Pressure, kb	Time, min	Starting material*	Products*
Mg_2SiO_4	TiO_2					
80	20	1790	10	3	En + Fo + M	L + Fo
80	20	1500	10	50	En + Fo + M	Q + Fo + M
80	20	1475	10	60	En + Fo + M	[En + Fo + M] + [((Q))]
70	30	1725	10	15	En + Fo + M	Q
70	30	1700	10	13	En + Fo + M	Q + Fo
70	30	1550	10	35	En + Fo + M	Q + Fo
70	30	1525	10	45	En + Fo + M	Q + Fo + M
70	30	1500	10	35	En + Fo + M	Q + Fo + M
70	30	1475	10	65	En + Fo + M	[En + Fo + M] + [((Q))]
60	40	1625	10	10	En + Fo + M	Q
60	40	1600	10	20	En + Fo + M	Q + Fo
60	40	1550	10	30	En + Fo + M	Q + Fo
60	40	1525	10	40	En + Fo + M	Q + Fo + M
60	40	1500	10	55	En + Fo + M	Q + Fo + M
60	40	1475	10	60	En + Fo + M	En + Fo + M
51	49	1575	10	10	P + Qz + Rt	Q
51	49	1550	10	5	P + Qz + Rt	Q + M
51	49	1530	10	7	P + Qz + Rt	Q + M
51	49	1510	10	25	P + Qz + Rt	Q + Fo + M
46.73	53.26	1550	10	30	En + M	Q + M
46.73	53.26	1500	10	40	En + M	Q + M
46.73	53.26	1475	10	50	En + M	En + M
43	57	1610	10	8	P + Qz + Rt	Q
43	57	1590	10	10	P + Qz + Rt	Q + M
43	57	1490	10	15	P + Qz + Rt	Q + M + En
43	57	1480	10	25	P + Qz + Rt	Q + M + En
43	57	1470	10	40	P + Qz + Rt	[En + M + Rt] + [(Q)]
40	60	1600	10	20	En + M + Rt	Q + M
40	60	1475	10	55	En + M + Rt	[Q + M] + [((En + M + Rt))]
40	60	1450	10	30	En + M + Rt	En + M + Rt
35	65	1650	10	5	P + Qz + Rt	Q
35	65	1630	10	5	P + Qz + Rt	Q + M
35	65	1550	10	15	P + Qz + Rt	Q + M + (Rt)
30	70	1675	10	7	En + M + Rt	Q
30	70	1650	10	11	En + M + Rt	Q + M
30	70	1625	10	12	En + M + Rt	Q + M + Rt
25	75	1690	10	4	En + M + Rt	Q
25	75	1670	10	7	En + M + Rt	Q + M + Rt
20	80	1700	10	6	En + M + Rt	Q + M ((Rt))
20	80	1675	10	7	En + M + Rt	Q + M + Rt
51	49	1575	15.5	10	P + Qz + Rt	Q + Fo
51	49	1550	15.5	15	P + Qz + Rt	Q + Fo + M
51	49	1510	15.5	15	P + Qz + Rt	Q + Fo + M
46.73	53.26	1550	15.5	10	En + M	Q + M + ((Fo))
43	57	1575	15.5	12	P + Qz + Rt	Q + M
43	57	1525	15.5	12	P + Qz + Rt	Q + M
43	57	1505	15.5	25	P + Qz + Rt	Q + M + (Fo)
40	60	1600	15.5	5	En + M + Rt	Q
40	60	1575	15.5	8	En + M + Rt	Q + M
40	60	1525	15.5	15	En + M + Rt	Q + M + (Rt)
40	60	1510	15.5	15	En + M + Rt	Q + M + Rt
35	65	1625	15.5	5	P + Qz + Rt	Q
35	65	1600	15.5	7	P + Qz + Rt	Q + Rt
35	65	1575	15.5	8	P + Qz + Rt	Q + M + (Rt)
35	65	1490	15.5	20	P + Qz + Rt	Fo + Rt
30	70	1625	15.5	7	En + M + Rt	Q + Rt
30	70	1600	15.5	7	En + M + Rt	Q + Rt
80	20	1855	20	3	En + M + Fo	Q + G
80	20	1842	20	3	En + M + Fo	Q + (Fo)
70	30	1770	20	13	En + M + Fo	Q
70	30	1745	20	10	En + M + Fo	Q + Fo
70	30	1580	20	10	En + M + Fo	Q + Fo
70	30	1570	20	35	En + M + Fo	Q + Fo + (M)
70	30	1525	20	40	En + M + Fo	[Fo + Rt] + [((Q))]
60	40	1700	20	10	En + M + Fo	Q + ((Fo))
60	40	1680	20	13	En + M + Fo	Q + Fo
60	40	1590	20	10	En + M + Fo	Q + Fo
60	40	1570	20	10	En + M + Fo	Q + Fo + (M)

TABLE 3 (continued)

Composition, weight percent		Temp, °C	Pressure, kb	Time, min	Starting material*	Products*
Mg_2SiO_4	TiO_2					
51	49	1590	20	10	P + Qz + Rt	Q + Fo
51	49	1575	20	10	P + Qz + Rt	Q + Fo + (M)
46.73	53.26	1625	20	25	En + M	Q
46.73	53.26	1600	20	25	En + M	Q + ((Fo))
46.73	53.26	1575	20	25	En + M	Q + Fo + (M)
46.73	53.26	1550	20	45	En + M	[Fo + Rt] + [((Q))]
43	57	1635	20	5	P + Qz + Rt	Q
43	57	1615	20	5	P + Qz + Rt	Q + M
43	57	1560	20	9	P + Qz + Rt	[L + Fo] + [((Fo + Rt))]
40	60	1625	20	23	En + M + Rt	Q + ((M))
40	60	1600	20	20	En + M + Rt	Q + M
40	60	1575	20	20	En + M + Rt	Q + M + Rt
40	60	1550	20	30	En + M + Rt	[Fo + Rt] + [((Q))]
35	65	1650	20	5	P + Qz + Rt	Q
35	65	1625	20	2	P + Qz + Rt	Q + Rt + (M)
30	70	1695	20	10	En + M + Rt	Q
30	70	1680	20	10	En + M + Rt	Q + (Rt)
30	70	1645	20	10	En + M + Rt	Q + Rt + M
25	75	1750	20	3-1/2	En + M + Rt	Q
25	75	1725	20	3	En + M + Rt	Q + Rt
25	75	1650	20	5	En + M + Rt	Q + Rt
25	75	1625	20	6	En + M + Rt	Q + Rt + (M)
20	80	1800	20	3	En + M + Rt	Q
20	80	1775	20	4	En + M + Rt	Q + Rt
20	80	1675	20	7	En + M + Rt	Q + Rt
20	80	1650	20	7	En + M + Rt	Q + Rt + ((M))
20	80	1625	20	10	En + M + Rt	Q + Rt + (M)
51	49	1725	40	3	P + Qz + Rt	Q
51	49	1700	40	3	P + Qz + Rt	Q + Fo
46.73	53.26	1675	40	4	En + M	Q
46.73	53.26	1665	40	5	En + M	Q + Fo
46.73	53.26	1650	40	5	En + M	Fo + Rt
43	57	1700	40	3	P + Qz + Rt	Q
43	57	1675	40	3	P + Qz + Rt	Q + Rt
43	57	1650	40	3	P + Qz + Rt	Fo + Rt
40	60	1725	40	3	En + M + Rt	Q
40	60	1700	40	3	En + M + Rt	Q + Rt
40	60	1675	40	10	En + M + Rt	Q + Rt
40	60	1660	40	5	En + M + Rt	Q + Rt
40	60	1635	40	13	En + M + Rt	Fo + Rt

*Abbreviations: P, periclase; Qz, quartz, coesite; Fo, forsterite; En, enstatite; M, magnesium titanate; Rt, rutile; Q, quench crystals; G, glass; parentheses indicate minor amounts; double parentheses indicate trace amounts; underline indicates subsolidus assemblage; square brackets indicate different phase assemblages in single experimental product, result of thermal gradient in capsule.

Additional evidence of the influence of pressure on the TiO_2 content in basalts is given by Kuno (1959). He has found a geographic correlation between the distribution of the Cenozoic tholeiite and alkaline olivine basalt provinces of Japan and the distribution of present day earthquakes having intermediate to deep foci. Kuno suggests that there is a close relationship between earthquake generation and the depth and mechanism of magma production. The earthquakes of shallow to intermediate depth underlie the tholeiitic province, and the deep earthquakes underlie the alkali-basalt province. The TiO_2 content of the tholeiitic rocks and alkali olivine basalt rocks shows widely different distributions. The alkali olivine basalts have a TiO_2 content approximately twice that of the tholeiitic basalts; that is, the TiO_2-rich basaltic rocks come from greater depths.

TABLE 4

Experimental results on the join $MgSiO_3$-$MgTi_2O_5$

Composition, weight percent		Temp, °C	Pressure, kb	Time, min	Starting material*	Products*
$MgSiO_3$	$MgTi_2O_5$					
90	10	1645	10	10	P + Qz + Rt	G
90	10	1625	10	10	P + Qz + Rt	Q + En
90	10	1605	10	10	P + Qz + Rt	Q + En + Fo
80	20	1600	10	10	P + Qz + Rt	Q
80	20	1580	10	10	P + Qz + Rt	Q + En + Fo
66.74	33.26	1575	10	25	G + Q	Q + ((Fo))
66.74	33.26	1550	10	25	G + Q	Q + Fo + (En)
53.93	46.07	1545	10	25	G + Q	Q
53.93	46.07	1525	10	20	G + Q	Q + Fo + (En)
42.94	57.06	1525	10	30	En + M	Q
42.94	57.06	1500	10	35	En + M	Q + Fo + (M)
42.94	57.06	1475	10	35	En + M	En + M
37	63	1570	10	10	P + Qz + Rt	Q
37	63	1550	10	10	P + Qz + Rt	Q + M
37	63	1515	10	10	P + Qz + Rt	Q + M
37	63	1495	10	10	P + Qz + Rt	Q + Fo + M
33.3	66.7	1525	10	35	En + M	Q + M
33.3	66.7	1500	10	40	En + M	Q + M + ((Fo))
33.3	66.7	1475	10	50	En + M	En + M
15	85	1695	10	5	En + M	Q + G
15	85	1675	10	7	En + M	Q + M
53.93	46.07	1525	15.5	15	G + Q	Q + Fo + En
53.93	46.07	1500	15.5	20	G + Q	[Fo + En + Rt] + [Q + Fo + En]
51.3	48.7	1520	15.5	20	P + Qz + Rt	Q + Fo
51.3	48.7	1505	15.5	20	P + Qz + Rt	Q + Fo + (En)
51.3	48.7	1490	15.5	20	P + Qz + Rt	Fo + En + Rt
48	52	1520	15.5	20	P + Qz + Rt	Q + (Fo)
48	52	1510	15.5	20	P + Qz + Rt	Q + Fo + ((M))
48	52	1495	15.5	20	P + Qz + Rt	[Fo + En + Rt] + [(Q) + (En) + (Fo)]
42.94	57.06	1550	15.5	15	En + M	Q + Fo
42.94	57.06	1530	15.5	20	En + M	Q + Fo + ((Mg))
42.94	57.06	1515	15.5	20	En + M	Q + Fo + M
42.94	57.06	1500	15.5	20	En + M	[Fo + En + Rt] + [Q + Rt + En] + [Q + M + Fo]
42.94	57.06	1490	15.5	20	En + M	Fo + En + Rt
37	63	1575	15.5	10	P + Qz + Rt	Q
37	63	1550	15.5	12	P + Qz + Rt	Q + M
37	63	1525	15.5	15	P + Qz + Rt	Q + M
37	63	1500	15.5	20	P + Qz + Rt	[Fo + En + Rt] + [Q + En + Rt] + [Q + Fo + M]
37	63	1495	15.5	20	P + Qz + Rt	Fo + En + Rt
33.3	66.7	1575	15.5	12	En + M	Q + M
33.3	66.7	1550	15.5	10	En + M	Q + M + (Fo)
33.3	66.7	1525	15.5	12	En + M	Q + M + Fo
25	75	1550	15.5	15	En + M	Q + M
25	75	1525	15.5	15	En + M	Q + M + (Fo)
25	75	1510	15.5	20	En + M	Q + M + Fo
80	20	1700	20	3	P + Qz + Rt	Q
80	20	1680	20	3	P + Qz + Rt	Q + En
80	20	1655	20	5	P + Qz + Rt	Q + Fo + En
66.74	33.26	1675	20	15	G + Q	Q
66.74	33.26	1650	20	10	G + Q	Q + En + (Fo)
66.74	33.26	1550	20	25	G + Q	Q + Fo + (En)
53.93	46.07	1650	20	10	G + Q	Q
53.93	46.07	1620	20	14	G + Q	Q + Fo + ((En))
53.93	46.07	1600	20	20	G + Q	Q + Fo + En
53.93	46.07	1550	20	55	G + Q	Q + Fo + En
53.93	46.07	1525	20	25	G + Q	Fo + En + Rt
42.94	57.06	1600	20	20	En + M	Q + (Fo)
42.94	57.06	1575	20	30	En + M	Q + (Fo)
42.94	57.06	1550	20	45	En + M	[Q + Fo] + [(Fo + En + Rt)]
42.94	57.06	1525	20	30	En + M	Fo + En + Rt
37	63	1600	20	15	P + Qz + Rt	Q + ((Fo))
37	63	1575	20	20	P + Qz + Rt	Q + Fo
37	63	1550	20	25	P + Qz + Rt	Q + Fo + (Rt)
37	63	1525	20	30	P + Qz + Rt	Fo + En + Rt
33.3	66.7	1625	20	25	En + M	Q

TABLE 4 (continued)

Composition, weight percent		Temp, °C	Pressure, kb	Time, min	Starting material*	Products*
$MgSiO_3$	$MgTi_2O_5$					
33.3	66.7	1600	20	25	En + M	Q + ((Fo))
33.3	66.7	1575	20	25	En + M	Q + Fo + (M)
33.3	66.7	1550	20	45	En + M	[Fo + Rt] + [((Q))]
25	75	1700	20	5	En + M	Q
25	75	1650	20	5	En + M	Q + M
25	75	1600	20	15	En + M	Q + M
25	75	1575	20	20	En + M	Q + M + (Fo)
25	75	1550	20	20	En + M	Fo + M + Rt
25	75	1525	20	25	En + M	Fo + M + Rt
15	85	1750	20	5	En + M	Q
15	85	1725	20	3	En + M	Q + ((M))
15	85	1600	20	10	En + M	Q + M
15	85	1575	20	15	En + M	Q + M + ((Fo))
15	85	1550	20	10	En + M	Fo + M + Rt
53.93	47.07	1750	40	3	G + Q	Q
53.93	47.07	1725	40	3	G + Q	Q + Fo
53.93	47.07	1700	40	3	G + Q	Q + Fo + En
42.94	57.06	1715	40	3	En + M	Q
42.94	57.06	1675	40	3	En + M	Q + Fo
42.94	57.06	1655	40	3	En + M	Q + Fo + (En)
37	63	1700	40	3	P + Qz + Rt	Q
37	63	1675	40	2	P + Qz + Rt	Q + Fo
37	63	1650	40	3	P + Qz + Rt	Q + Fo + (Rt)
37	63	1630	40	5	P + Qz + Rt	Fo + Rt + En
33.3	66.7	1675	40	4	En + M	Q
33.3	66.7	1665	40	5	En + M	Q + Fo
33.3	66.7	1650	40	5	En + M	Fo + Rt
25	75	1750	40	3	En + M	Q
25	75	1725	40	3	En + M	Q + M
25	75	1670	40	3	En + M	Q + M
25	75	1650	40	5	En + M	Q + M + Fo
25	75	1640	40	8	En + M	[Fo + Rt + M] + [(Q)]

*Abbreviations: P, periclase; Qz, quartz, coesite; Fo, forsterite; En, enstatite; M, magnesium titanate; Rt, rutile; Q, quench crystals; G, glass; parentheses indicate minor amounts; double parentheses indicate trace amounts; underline indicates subsolidus assemblage; square brackets indicate different phase assemblages in single experimental product, result of thermal gradient in capsule.

The question now arises as to whether the TiO_2-rich basalts may in general be correlated with alkaline basalts and the TiO_2-poor basalts with sub-alkaline (Chayes, 1966) basalts. Experimental data on several ternary systems (Kushiro, 1968) indicate that subalkaline basalts may form down to depths of approximately 90 km and that alkaline basalts are derived from the depth range 30 to 130 km. Partial melting experiments on natural basalt compositions give a similar result (Green and Ringwood, 1967). Subalkaline basalts may be derived at all depths down to approximately 130 km, whereas alkaline basalts are formed in the approximate depth range 30 to 60 km. Thus the current experimental data indicates that only the subalkaline basalts are derived from depths less than 30 km, and both subalkaline and alkaline basalts can be derived from greater depths. Heat flow considerations mitigate against an origin by partial fusion at depths less than 30 km indicating that subalkaline basalts derived from this zone are the products of fractional crystallization in temporary magma chambers. Both Yoder and Tilley (1962) and Green and Ringwood (1967) concluded that alkaline basalts may be derived from subalkaline basalts at greater depths by fractional crystal-

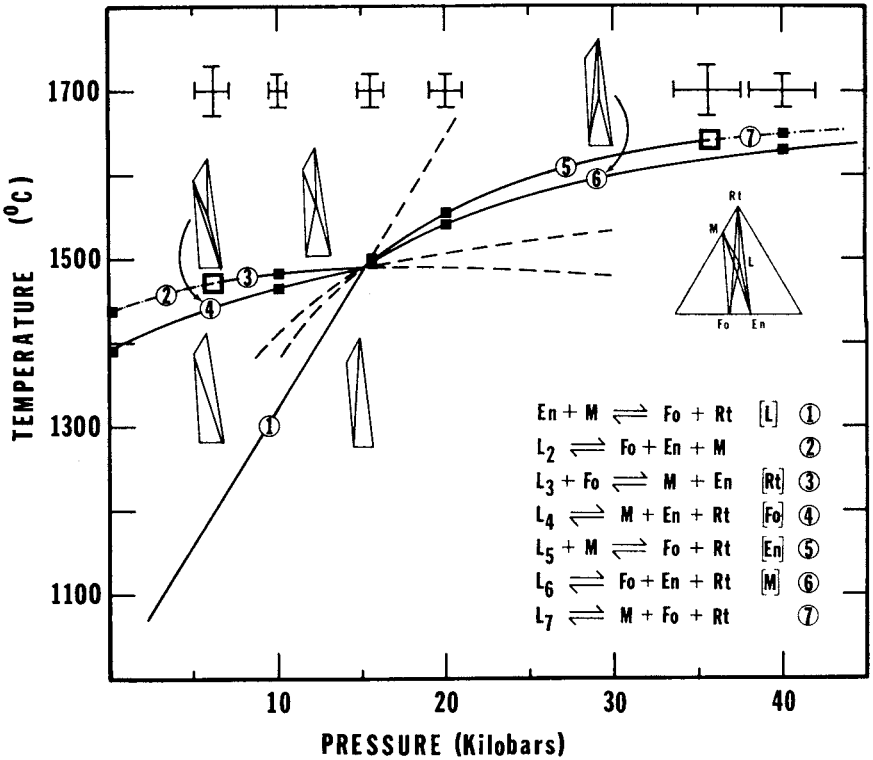

Fig. 5. Temperature-pressure section showing univariant equilibria for reactions (1) through (7). Solid curves give stable portions of univariant reactions that intersect at the invariant point; dashed curves give metastable extensions; dash-dot curves are for reactions (2) and (7) which do not intersect at the invariant point. Solid squares give data points; open squares give interpolated data points (table 6). Error bars at 1700°C give estimated errors for each pressure where data are available. Invariant liquid composition used in phase diagrams.

lization. At these greater depths, they may also be produced by partial fusion of an ultramafic mantle (Green and Ringwood, 1967; O'Hara and Yoder, 1967), with alkaline basalt representing a smaller proportion of partial fusion than the subalkaline basalts.

Chayes and Velde (1965) show that their oceanic island suite is composed of a mixture of alkaline and subalkaline basalts whereas the circumoceanic basalts are nearly all subalkaline. Also, they note that both the subalkaline and alkaline basalts from oceanic islands are TiO_2-rich while the subalkaline circumoceanic basalts are TiO_2-poor. If we conclude, from the present experimental work, that the TiO_2 content of any basaltic rock increases with increasing depth of origin, then the subalkaline basalts must be derived from a range of depths both shallow and deep, while the alkaline basalts are derived only from greater depths. This conclusion is in essential agreement with other experimental data and adds further confirmation that pressure is an important variable in the determination of the compositions of basalts.

TABLE 5

Experimental results from compositions in the ternary MgO-SiO_2-TiO_2

Composition, weight percent			Temp, °C	Pressure, kb	Time, min	Starting material*	Products*
MgO	SiO_2	TiO_2					
25.4	33.4	41.2	1490	10	10	P + Qz + Rt	Q + En
25.4	33.4	41.2	1485	10	10	P + Qz + Rt	Q + En + (M)
25.4	33.4	41.2	1475	10	30	P + Qz + Rt	[Q + En + M] + [En + M + Rt]
24.4	32.6	43.0	1480	10	20	P + Qz + Rt	[Q] + [Q + Rt] + [Q + Rt + En] + [En + M + Rt]
25.4	33.4	41.2	1520	15.5	20	P + Qz + Rt	Q + En + Rt
25.4	33.4	41.2	1535	15.5	15	P + Qz + Rt	Q + ((En))
24.4	32.6	43.0	1535	15.5	15	P + Qz + Rt	Q + (Rt)
24.6	23.4	52.0	1535	15.5	20	P + Qz + Rt	Q
24.6	23.4	52.0	1528	15.5	20	P + Qz + Rt	Q + Rt
24.6	23.4	52.0	1520	15.5	20	P + Qz + Rt	Q + M + Rt
25.8	24.2	50.0	1550	15.5	15	P + Qz + Rt	Q + M
25.8	24.2	50.0	1540	15.5	15	P + Qz + Rt	Q + M + Fo
25.8	24.2	50.0	1560	20	10	P + Qz + Rt	Q + (Fo)
25.8	24.2	50.0	1550	20	10	P + Qz + Rt	Q + Fo + Rt
24.6	23.4	52.0	1550	20	20	P + Qz + Rt	Q + (Rt)
25.7	18.4	55.8	1657	40	5	P + Qz + Rt	Q + ((Fo))
25.7	18.4	55.8	1645	40	5	P + Qz + Rt	Q + Fo + M
25.7	22.2	52.1	1655	40	1	P + Qz + Rt	Q + (Fo)
25.8	24.2	50.0	1660	40	5	P + Qz + Rt	Q
25.8	24.2	50.0	1665	40	5	P + Qz + Rt	Q + (En)
25.8	24.2	50.0	1650	40	5	P + Qz + Rt	Fo + En + Rt
25.0	18.0	57.0	1665	40	5	P + Qz + Rt	Q + (M)
25.0	18.0	57.0	1655	40	5	P + Qz + Rt	Q + M + Rt
25.0	22.0	53.0	1660	40	5	P + Qz + Rt	Q
25.0	22.0	53.0	1654	40	5	P + Qz + Rt	Q + Rt
25.0	22.0	53.0	1645	40	5	P + Qz + Rt	Q + Rt + En
24.4	32.6	43.0	1675	40	5	P + Qz + Rt	Q + En

*Abbreviations: P, periclase; Qz, quartz, coesite; Fo, forsterite; En, enstatite; M, magnesium titanate; Rt, rutile; Q, quench crystals; parentheses indicate minor amounts; double parentheses indicate trace amounts; underline indicates subsolidus assemblage; square brackets indicate different phase assemblages in single experimental product, result of thermal gradient in capsule.

TABLE 6

Experimentally determined compositions and temperatures of eutectic and peritectic liquids in the phase region Mg_2SiO_4-$MgSiO_3$-TiO_2-$MgTi_2O_5$

Ternary liquids	Pressure	Temp, °C	Weight percent		
			MgO	SiO_2	TiO_2
Eutectic (E_2)	1 atm	1440	33.6	32.4	34.0
Eutectic (E_4)	1 atm	1390	31.5	35.7	32.8
Eutectic (E_2^x)*	6.4 kb	1473	30.0	28.0	42.5
Peritectic (P_3)	10 kb	1485	28.5	27.1	44.4
Eutectic (E_4)	10 kb	1465	24.9	32.7	42.4
Invariant point	15.2 kb	1489	26.0	27.0	47.0
Peritectic (P_5)	15.5 kb	1494	25.8	26.2	48.0
Eutectic (E_6)	15.5 kb	1491	25.8	26.7	47.5
Peritectic (P_5)	20 kb	1555	25.3	21.8	52.9
Eutectic (E_6)	20 kb	1540	25.2	24.4	50.4
Peritectic (P_5^x)*	35.6 kb	1641	25.5	19.0	55.5
Eutectic (E_6)	40 kb	1650	25.6	22.2	52.2
Eutectic (E_7)	40 kb	1630	25.6	18.5	55.9

*Data points obtained by linear interpolation; eutectic (E_2^x) and peritectic (P_5^x) give the pressures, temperatures, and compositions at which the 1 atm eutectic (E_2) (fig. 4A) and the 20 kb peritectic (P_5) (fig. 4C) convert, with increasing pressure, to the peritectic (P_4) (fig. 4B) and eutectic (E_7) (fig. 4E), respectively.

It would appear that the TiO_2 content of a basalt increases with pressure independent of degree of alkalinity (Chayes, 1966) and is thus a particularly useful indicator of depth of origin. With reference to Chayes and Velde's (1965) success in discriminating between basalts of different geographical origins, the present results indicate that the tectonic setting is more critical than geography in determining the chemistry of a basalt. The results imply that the magma reservoirs which give rise to circumoceanic basalts are at shallower depths than those for oceanic island basalts.

ACKNOWLEDGMENTS

The work for this paper was started while the author was a fellow at the Geophysical Laboratory. The Chayes (1964) and Chayes and Velde (1965) observations of the importance of TiO_2 as a geographic discriminator for basaltic rocks stimulated the study of a simple basalt system with TiO_2 as a component.

The experiments forming the basis of this report have been made at the Geophysical Laboratory (MacGregor, 1965b) and at the Southwest Center for Advanced Studies. The author is indebted to Dr. F. R. Boyd for the use of the high-pressure equipment, and to Dr. P. M. Bell and Dr. D. Lindsley for their advice and assistance. Dr. J. F. Schairer assisted greatly in making the starting compositions; the amiable availability of his time, equipment, and advice is much appreciated. D. Martin helped considerably in making the experiments. His concientious, intelligent, and good-natured help is much appreciated.

Drs. F. R. Boyd, P. M. Bell, D. Lindsley, J. W. Graham, J. L. Carter, and D. Presnall have read the manuscript and given advice which has significantly improved the paper. Dr. Presnall has helped in many discussions to clarify the author's ideas and improve the presentation.

The experimental work and final writing of the report was done at the Southwest Center for Advanced Studies with the financial support of the National Aeronautics and Space Administration contract NsG-269-62. This support is gratefully appreciated.

APPENDIX

EXPERIMENTAL PROCEDURE

Apparatus.—The experiments were conducted in a solid-media, piston-cylinder device (Boyd, 1962), with a solid-media furnace assembly constructed following the techniques of Boyd and England (1963).

Experimental uncertainties.—In all the experiments of this study, the sample was first raised to a pressure of 2 kb in excess of that required for the experiment. The piston was then retracted to the required pressure, and the temperature raised to the required temperature. This procedure was adopted to compensate, approximately, for the piston-cylinder friction, so that the gauge pressure gave, within the error limits, the pressure of the experiment. Subsequent minor adjustments due to changes in temperature were made to keep the pressure constant during the experiment. Following Newton and Smith's (1967) experience and assuming a symmetrical friction correction, retracting the piston by 2 kb leads to corrections of approximately $+10$, $+3$, 0, and -5 percent at 10, 15.5, 20, and 40 kb total pressure, respectively. However, considering the variable nature of the friction correction from experiment to experiment (Boyd, Bell, England, and Gilbert, 1966) the prediction of an exact pressure correction for each experiment is not possible. By following the above procedure all the observed gauge pressures, recorded in the table of results,

are probably correct to within ±10 percent with most values falling within ±5 percent.

Temperatures uncertainties in the solid-media apparatus arise from three sources. A small unknown pressure correction on the thermocouple (Hanneman and Strong, 1965; Bell, England, and Boyd, 1967), lag in the temperature control system, and thermal gradients in the furnace assembly (Boyd and England, 1963) all contribute to the temperature uncertainty. No data are currently available to evaluate the pressure effect on the emf generated by a Pt–$Pt_{90}Rh_{10}$ thermocouple in the temperature-pressure range of the present experiments; corrections must wait till these data are available. Temperature lag in the electronic control circuit is of the order of ±5°C. Experimentally determined thermal gradients across the capsule are less than 10°C at 1400°C and increase to a maximum of 15°C at 1800°C. It is estimated that the recorded temperatures are correct to within ±10°C.

All samples were quenched by cutting power to the graphite resistance furnace. For an experiment at 1750°C the sample quenched to 1000°C in 3 seconds and to 300°C in 9 seconds.

Starting materials.—The starting materials were made from MgO, TiO_2, and SiO_2. The MgO was made from 99.995 percent pure Mg metal, dissolved in reagent grade nitric acid and fired at 1100°C to convert the nitrates to oxides. The TiO_2 was Fisher, reagent grade, material, and the SiO_2 was from the same batch as that used by Schreyer and Schairer (1961). Before weighing out the various mixes, MgO was fired at 1200°C for 1 hour and then at 1500°C for 12 hours; TiO_2 and SiO_2 were dried at 1200°C for 4 hours. The products from the drying procedures were periclase, rutile, and trydimite for MgO, TiO_2, and SiO_2, respectively.

For each composition, 5 g total of oxides was weighed into an agate mortar and ground under alcohol for 40 minutes. Three procedures were then followed. Those compositions with 1 atm liquidus temperatures (Massazza and Sirchia, 1958b) below 1500°C were held at 1570°C for 4 hours and then quenched to a mixture of glass and minor amounts of quench crystals. Mixtures with 1 atm liquidus temperatures above 1500°C were held at 1250°C for 48 hours and recrystallized to their 1 atm subsolidus assemblages (Massazza and Sirchia, 1958b). In both the above cases the samples were reground and refired twice, in order to homogenize more completely the sample. Some compositions were left as unreacted mixtures of the original oxides.

The specific starting materials used for each experiment are listed in tables 1 through 5. The various starting materials give a coherent pattern of results, and it has been assumed that this pattern represents equilibrium. The starting materials and furnace parts were dried at 1000°C in dry nitrogen for 40 minutes. All the results shown were made in graphite capsules; however, a number of duplicate runs in platinum capsules gave identical results.

Examination of products.—All experimental products were first examined with a binocular microscope. Subsequently, the crushed products were examined in immersion oils with a petrographic microscope. In general it was possible to identify all the phases with the petrographic microscope; X-ray diffractograms were used as an aid in verifying the optical identifications. The only phases present in the portion of the system examined are forsterite (Mg_2SiO_4), enstatite ($MgSiO_3$), magnesium titanate ($MgTi_2O_5$), giekielite ($MgTiO_3$), rutile (TiO_2), and liquid.

Subsolidus aggregates of those phases that had grain sizes in the range 3 to 10 mu were satisfactorily identified only with X-ray techniques. Because of grain sizes in the range 10 to 150 mu, the crystal-liquid mixtures were more amendable to optical identification. Glass and quench crystals were readily identifiable, although considerable difficulty was initially experienced in recognizing the very coarse $MgTi_2O_5$ quench crystals commonly found in the TiO_2-rich compositions. When occurring with quench crystals or glass, the enstatite formed euhedral to subhedral tabular crystals of low birefringence (first order gray); the olivine formed equant crystals, commonly with hexagonal outlines, and had an intermediate birefringence (first order yellow); the magnesium titante formed translucent, National blue (44-B-1, Maerz and Paul, 1930), rectangular crystals with very low birefringence, and the rutile formed stubby, blue (44-R-12, Maerz and Paul, 1930), rod-like crystals. It is thought that the blue color is due to an oxygen deficiency in the rutile structure. However, no magneli phases were observed, and the lack of any observed non-ternary behavior suggests that the experimental results may be considered as essentially ternary. In general, the intensity of the blue color in the rutile increased with increasing temperature. Because of the thermal gradients in the capsule, binocular microscope examination

was essential in the interpretation of experiments, whose conditions straddled more than one phase field and for those cases where a composition had a phase field with a stability range of less than 20°C.

For all the isobaric sections, the data of Boyd, England, and Davis (1964) and Davis and England (1964) were used for the melting temperatures of enstatite ($MgSiO_3$) and forsterite (Mg_2SiO_4), respectively.

References

Bell, P. M., England, J. L., and Boyd, F. R., 1967, Pressure effect on the platinum versus platinum 10% rhodium thermocouple; Carnegie Inst. Washington Year Book 66, p. 545-547.

Boyd, F. R., 1962, Phase equilibria in silicate syystems at high pressures and temperatures, *in* Wentorf, R. W., Jr., ed., Modern very high pressure techniques: Washington, Butterworths, p. 151-162.

Boyd, F. R., Bell, D. M., England, J. L., and Gilbert, M. C., 1966, Pressure measurement in single-stage apparatus: Carnegie Inst. Washington Year Book 65, p. 410-414.

Boyd, F. R., and England, J. L., 1960, Apparatus for phase-equilibrium measurements at pressures up to 50 kilobars and temperatures up to 1750°C; Jour. Geophys. Research, v. 65, p. 741-748.

———— 1963, Effect of pressure on the melting of diopside, $CaMgSi_2O_6$, and albite, $NaAlSi_3O_8$, in the range up to 50 kilobars: Jour. Geophys. Research, v. 68, p. 311-323.

Boyd, F. R., England, J. L., and Davis, B. T. C., 1964, Effects of pressure on the melting and polymorphism of enstatite, $MgSiO_3$: Jour. Geophys. Research, v. 69, p. 2101-2109.

Carter, J. L., 1966, Chemical composition of the primitive upper mantle [abs.]: Geol. Soc. America, Spec. Paper 101, p. 35-36.

Chayes, Felix, 1964, A petrographic distinction between Cenozoic volcanics in and around the open oceans: Jour. Geophys. Research, v. 69, p. 1573-1588.

———— 1966, Alkaline and subalkaline basalts: Am. Jour. Sci., v. 264, p. 128.

Chayes, Felix, and Velde, D., 1965, On distinguishing basaltic lavas of circumoceanic and oceanic-island type by means of discriminant functions: Am. Jour. Sci., v. 263, p. 206-222.

Davis, B. T. C., and England, J. L., 1964, The melting of forsterite up to 50 kilobars: Jour. Geophys. Research, v. 69, p. 1113-1116.

Green, D. H., and Ringwood, A. E., 1963, Mineral assemblages in a model composition: Jour. Geophys. Research, v. 68, p. 937-946.

———— 1967, Genesis of basaltic magmas: Contr. Mineralogy Petrology, v. 15, p. 103-190.

Hanneman, R. E., and Strong, H. M., 1965, Pressure dependence of the emf of thermocouples to 1300°C and 50 K bar: Jour. Appl. Physics, v. 36, p. 523-528.

Harris, P. G., Reay, A., and White, I. G., 1967, Chemical composition of the Upper Mantle: Jour Geophys. Research, v. 72, p. 6359-6369.

Hess, H. H., 1964, The oceanic crust, the upper mantle and the Mayaguez serpentinized peridotite: Natl. Assoc. Sci.-Research Council Pub. 1188, p. 169-175.

Ito, K., and Kennedy, G. C., 1967, Melting and phase relations in a natural peridotite to 40 kilobars: Am. Jour. Sci., v. 265, p. 519-538.

Kuno, H., 1959, Origin of Cenozoic petrographic provinces of Japan and surrounding area: Bull. volcanologique, 2nd ser., v. 20, p. 37-76.

Kushiro, I., 1968, Compositions of magmas formed by partial zone melting of the Earth's Upper Mantle: Jour. Geophys. Research, v. 7, p. 619-634.

MacGregor, I. D., 1965a, Stability fields of spinel and garnet peridotites in the synthetic system MgO–CaO–Al_2O_3–SiO_2: Carnegie Inst. Washington Year Book 64, p. 127-134.

———— 1965b, The effect of pressure on the minimum melting composition in the system Mgo–SiO_2–TiO_2: Carnegie Inst. Washington Year Book 64, p. 135-139.

Maerz, A., and Paul, M. R., 1930, A dictionary of color: New York, McGraw Hill Book Co.

Massazza, F., and Sirchia, E., 1958a, Il sistema MgO–SiO_2–TiO_2: Nota I-Revisione dei sistemi binari; Chim Ind. (Milan), v. 40, p. 376-380.

———— 1958b, Il sistema Mgo–SiO_2–TiO_2: Nota II-Gli equilibri alto stato solido e alla fusione; Chim. Ind. (Milan), v. 40, p. 460-467.

Newton, R. C., and Smith, J. V., 1967, Investigations concerning the breakdown of albite at depth in the earth: Jour. Geology, v. 75, p. 268-286.

O'Hara, M. J., and Yoder, H. S., 1967, Formation and fractionation of basic magmas at high pressures; Scottish Jour. Geology, v. 3, pt. 1, p. 67-117.

Ringwood, A. E., 1966, The chemical composition and origin of the earth, *in* Hurley, P. M., ed., Advances in Earth Sciences: Cambridge, Mass., M. I. T. Press., p. 287-356.

Schreyer, W., and Schairer, J. F., 1961, Compositions and structural states of anhydrous Mg-cordierites: A reinvestigation of the central part of the system MgO–Al_2O_3–SiO_2: Jour. Petrology, v. 2, p. 324-406.

Yoder, H. S., and Tilley, C. E., 1962, Origin of basaltic magmas; An experimental study of natural and synthetic rock systems: Jour. Petrology, v. 3, p. 342-532.